Monthly Notices of the ROYAL ASTRONOMICAL SOCIETY

MNRAS **437,** 1681–1697 (2014) doi:10.1093/mnras/stt2007
Advance Access publication 2013 November 20

EL CVn-type binaries – discovery of 17 helium white dwarf precursors in bright eclipsing binary star systems

P. F. L. Maxted,[1]⋆ S. Bloemen,[2] U. Heber,[3] S. Geier,[3,4] P. J. Wheatley,[5] T. R. Marsh,[5] E. Breedt,[5] D. Sebastian,[6] G. Faillace,[7] C. Owen,[7] D. Pulley,[7] D. Smith,[7] U. Kolb,[7] C. A. Haswell,[7] J. Southworth,[1] D. R. Anderson,[1] B. Smalley,[1] A. Collier Cameron,[8] L. Hebb,[9] E. K. Simpson,[10] R. G. West,[5] J. Bochinski,[7] R. Busuttil[7] and S. Hadigal[7,11]

[1]*Astrophysics Group, Keele University, Keele, Staffordshire ST5 5BG, UK*
[2]*Instituut voor Sterrenkunde, University of Leuven, Celestijnenlaan 200D, B-3001 Heverlee, Belgium*
[3]*Dr. Karl Remeis-Observatory & ECAP, Sternwartstr. 7, D-96049 Bamberg, Germany*
[4]*European Southern Observatory, Karl-Schwarzschild-Str. 2, D-85748 Garching, Germany*
[5]*Department of Physics, University of Warwick, Coventry CV4 7AL, UK*
[6]*Thüringer Landessternwarte Tautenburg, Sternwarte 5, D-07778 Tautenburg, Germany*
[7]*Department of Physical Sciences, The Open University, Walton Hall, Milton Keynes MK7 6AA, UK*
[8]*SUPA, School of Physics & Astronomy, University of St Andrews, North Haugh, St Andrews, Fife KY16 9SS, UK*
[9]*Department of Physics and Astronomy, Vanderbilt University, Nashville, TN 37235, USA*
[10]*Astrophysics Research Centre, School of Mathematics & Physics, Queen's University Belfast, Belfast BT7 1NN, UK*
[11]*International Space University, 1 rue Jean-Dominique Cassini, F-67400 Illkirch-Graffenstaden, France*

Accepted 2013 October 16. Received 2013 October 16; in original form 2013 July 24

ABSTRACT

The star 1SWASP J024743.37−251549.2 was recently discovered to be a binary star in which an A-type dwarf star eclipses the remnant of a disrupted red giant star (WASP 0247−25 B). The remnant is in a rarely observed state evolving to higher effective temperatures at nearly constant luminosity prior to becoming a very low mass white dwarf composed almost entirely of helium, i.e. it is a pre-helium white dwarf (pre-He-WD). We have used the photometric database from the Wide Angle Search for Planets (WASP) to find 17 eclipsing binary stars with orbital periods $P = 0.7$–2.2 d with similar light curves to 1SWASP J024743.37−251549.2. The only star in this group previously identified as a variable star is the brightest one, EL CVn, which we adopt as the prototype for this class of eclipsing binary star. The characteristic light curves of EL CVn-type stars show a total eclipse by an A-type dwarf star of a smaller, hotter star and a secondary eclipse of comparable depth to the primary eclipse. We have used new spectroscopic observations for six of these systems to confirm that the companions to the A-type stars in these binaries have very low masses ($\approx$0.2 $M_{\odot}$). This includes the companion to EL CVn which was not previously known to be a pre-He-WD. EL CVn-type binary star systems will enable us to study the formation of very low mass white dwarfs in great detail, particularly in those cases where the pre-He-WD star shows non-radial pulsations similar to those recently discovered in WASP0247−25 B.

Key words: binaries: close – binaries: eclipsing – binaries: spectroscopic – stars: individual: 1SWASP J024743.37−251549.2 – stars: individual: EL CVn.

1 INTRODUCTION

1SWASP J024743.37−251549.2 (hereafter WASP 0247−25) is one of several million bright stars ($8 \lesssim V \lesssim 13$) that have been observed by the Wide Angle Search for Planets (WASP; Pollacco et al. 2006). Maxted et al. (2011) showed that this eclipsing binary star contains an A-type dwarf star (WASP 0247−25 A) and a pre-helium white dwarf (pre-He-WD) with a mass $\approx$0.2 $M_{\odot}$ (WASP 0247−25 B). The only other example of a similar eclipsing binary star known at that time was the star V209 in the globular cluster ω Cen (Kaluzny et al. 2007). This is an extremely unusual object in which a pre-He-WD is eclipsed by a 0.945 $M_{\odot}$ star with an effective temperature $T_{\rm eff} = 9370$ K. The eclipsing binary star AW UMa may also contain a pre-He-WD, although the interpretation of this system is complicated by an equatorial belt of material that makes the light

⋆E-mail: p.maxted@keele.ac.uk

curve of this binary look like that of a W UMa-type contact binary star (Pribulla & Rucinski 2008). More recently, Pietrzyński et al. (2012) have discovered that the star OGLE-BLG-RRLYR-02792 is an eclipsing binary star with an orbital period of 15.2 d in which a pre-He-WD star with a mass of $0.26\,M_{\odot}$ shows RR-Lyrae-type pulsations with a period of 0.63 d. Some very young helium white dwarfs (He-WD) in eclipsing binary systems have been identified using Kepler photometry (Rowe et al. 2010; van Kerkwijk et al. 2010; Carter, Rappaport & Fabrycky 2011; Breton et al. 2012). These stars are difficult to study because they are much fainter than their A-type and B-type companion stars. In contrast, HZ 22 (Schönberner 1978) and HD 188112 (Heber et al. 2003) are also known to be pre-He-WD, but the companions to these non-eclipsing binary stars are too faint to have been detected so far, and so it has not been possible to derive precise, model-independent masses for these stars.

Low-mass white dwarf stars ($M \lesssim 0.35\,M_{\odot}$) are the product of binary star evolution (Iben & Livio 1993; Marsh, Dhillon & Duck 1995). Various evolution channels exist, but they are generally the result of mass transfer from an evolved main-sequence star or red giant star on to a companion star. Towards the end of the mass transfer phase the donor star will have a degenerate helium core. This 'stripped red giant star' does not have sufficient mass to undergo a helium flash, and so the white dwarf that emerges has an anomalously low mass and is composed almost entirely of helium. For this reason, they are known as He-WD. If the companion to the red giant is a neutron star then the mass transfer is likely to be stable so the binary can go on to become a low-mass X-ray binary containing a millisecond pulsar. Several millisecond radio pulsars are observed to have low-mass white dwarf companions (Lorimer 2008). Many He-WD have been identified in the Sloan Digital Sky Survey (Kilic et al. 2007), some with masses as low as $0.16\,M_{\odot}$ (Kilic et al. 2012), and from proper motion surveys (Kawka & Vennes 2009). Searches for radio pulsar companions to these white dwarfs have so far found nothing, so the companion stars are likely to also be white dwarf stars (Agüeros et al. 2009). This can be confirmed in those few cases where these binary white dwarf pairs show eclipses (Brown et al. 2011; Parsons et al. 2011). He-WD can also be produced by mass transfer from a red giant on to a main-sequence star, either rapidly through unstable common-envelope evolution or after a longer-lived 'Algol' phase of stable mass transfer (Refsdal & Weigert 1969; Giannone & Giannuzzi 1970; Iben & Livio 1993; Nelson & Eggleton 2001; Chen & Han 2003; Willems & Kolb 2004). He-WDs may also be the result of collisions in dense stellar environments such as the cores of globular clusters (Knigge et al. 2008).

The evolution of He-WDs is expected to be very different from more massive white dwarfs. If the time-scale for mass loss from the red giant is longer than the thermal time-scale, then when mass transfer ends there will still be a thick layer of hydrogen surrounding the degenerate helium core. The mass of the hydrogen layer depends on the total mass and composition of the star (Nelson, Dubeau & MacCannell 2004), but is typically 0.001–$0.005\,M_{\odot}$, much greater than for typical white dwarfs (hydrogen layer mass $<10^{-4}\,M_{\odot}$). The pre-He-WD then evolves at nearly constant luminosity towards higher effective temperatures as a result of the gradual reduction in the hydrogen layer mass through stable p–p chain shell burning. This pre-He-WD phase can last several million years for lower mass stars with thicker hydrogen envelopes. Towards the end of this phase p–p chain fusion becomes less efficient and the star starts to fade and cool.

The smooth transition from a pre-He-WD to a He-WD can be interrupted by one or more phases of unstable CNO burning (shell flashes) for pre-He-WD with masses ≈0.2–$0.3\,M_{\odot}$ (Webbink 1975; Driebe et al. 1999). These shell flashes substantially reduce the mass of hydrogen that remains on the surface. The mass range within which shell flashes are predicted to occur depends on the assumed composition of the star and other details of the models (Althaus, Serenelli & Benvenuto 2001). The cooling time-scale for He-WD that do not undergo shell flashes is much longer than for those that do because their thick hydrogen envelopes can support residual p–p chain fusion for several Gyr.

Maxted et al. (2013) found strong observational support for the assumption that He-WD are born with thick hydrogen envelopes. They found that only models with thick hydrogen envelopes could simultaneously match their precise mass and radius estimates for both WASP 0247−25 A and WASP 0247−25 B, together with other observational constraints such as the orbital period and the likely composition of the stars based on their kinematics. In addition, they found that WASP 0247−25 B is a new type of variable star in which a mixture of radial and non-radial pulsations produces multiple frequencies in the light curve near 250 cycles d^{-1}. This opens up the prospect of using asteroseismology to study the interior of this star, e.g. to measure its internal rotation profile.

The study by Maxted et al. of WASP 0247−25 clearly demonstrates that finding a pre-He-WD in a bright eclipsing binary system makes it possible to study these rarely observed stars in great detail and so better understand all low-mass white dwarfs. This will, in turn, improve our understanding of the various exotic binary systems and extreme stellar environments in which low-mass white dwarfs are found. Motivated by this discovery, we have used the WASP photometric data base to search for similar eclipsing binary systems to WASP 0247−25. Here we present an analysis of the WASP light curves and other data for 17 new eclipsing binary stars, 16 of which are new discoveries, and all of which are newly identified as binary systems containing a pre-He-WD.

2 TARGET SELECTION

The WASP survey is described in Pollacco et al. (2006) and Wilson et al. (2008). The survey obtains images of the night sky using two arrays of eight cameras each equipped with a charge-coupled device (CCD), 200-mm f/1.8 lenses and a broad-band filter (400–700 nm). Two observations of each target field are obtained every 5–10 min using two 30 s exposures. The data from this survey are automatically processed and analysed in order to identify stars with light curves that contain transit-like features that may indicate the presence of a planetary companion. Light curves are generated using synthetic aperture photometry with an aperture radius of 48 arcsec. Data for this study were obtained between 2004 May 05 and 2011 August 02.

We identified stars with light curves similar to WASP 0257−25 in the WASP photometric archive by inspection of the light curves folded on orbital periods identified by the various transit detection algorithms used by this survey. We looked for a characteristic light curve in which the primary eclipse has a 'boxy' appearance, i.e. steep ingress and egress and a well-defined flat section, and the secondary eclipse due to the transit of the pre-He-WD has a comparable depth but is shallower than the total eclipse caused by the occultation. Stars were selected for inspection based on various combinations of parameters that characterized the phase-folded light curve, e.g. the depth and width of the eclipse.

For each star with this type of light curve we used a least-squares fit of a light-curve model and inspection of the available catalogue photometry similar to the final analysis described below to verify that the primary eclipse is due to the total eclipse by an A-type

Table 1. New EL CVn-type binary stars identified using the WASP archive. Spectral types are taken from the SIMBAD data base.

1SWASP	*P* (d)	*V*	Notes
J013129.76+280336.5	1.882	10.9	TYC 1755-509-1
J034623.68−215819.5	0.928	9.6	HD 23692, A4 IV
J035838.33−311638.3	2.189	11.4	CD−31 1621, A3
J084356.46−113327.5	0.793	10.7	TYC 5450-1192-1
J084558.78+530209.8	0.844	12.9	
J093957.74−191941.2	1.073	12.1	TYC 6051-1123-1
J100927.98+200519.4	1.395	12.3	
J102122.83−284139.6	0.901	11.1	TYC 6631-538-1
J132357.01+433555.4	0.795	9.4	EL CVn, A1 V
J142951.60−244327.4	2.173	10.8	HD 127051, F0
J162545.15−043027.9	1.526	10.4	HD 148070, A0
J162842.31+101416.7	0.720	12.9	
J181417.43+481117.0	1.798	10.7	TYC 3529-1515-1
J204746.49+043602.0	1.563	11.8	TYC 520-1173-1
J210129.26−062214.9	1.290	11.5	TYC 5204-1575-1
J224905.95−693401.8	1.162	12.5	TYC 9337-2511-1
J232812.74−395523.3	0.768	13.3	

or F-type dwarf star of a smaller, hotter star. We found 17 stars that satisfied these criteria, only one of which (EL CVn) has been previously catalogued as an eclipsing binary star. Although EL CVn was not previously known to contain a pre-He-WD, it is currently the brightest known example of this type of binary star and is the only one to-date with an entry in the General Catalogue of Variable Stars (Kazarovets et al. 2008). For these reasons, and as a matter of convenience, we choose EL CVn as the prototype of this class of variable star. The new EL CVn-type binary stars identified are listed in Table 1.

The new EL CVn stars presented here are not a complete survey of the WASP archive for this type of binary star. The selection effects that affect this incomplete survey of the WASP archive may be large and are difficult to quantify. For example, WASP 0845+53 was included in this study because the lead author noticed a print-out of its light curve on a co-author's desk.

3 ADDITIONAL OBSERVATIONS

3.1 PIRATE photometry

Observations of WASP 1628+10 were obtained with the 0.4-m PIRATE telescope (Holmes et al. 2011) using the R filter and an exposure time of 30 s on various nights from 2012 June 18 to 2012 August 14. The facility, located at the Observatorio Astronòmico de Mallorca (OAM) at 200-m altitude, was set up in its PIRATE Mk II configuration. This comprises a 17-inch PlaneWave CDK telescope with focal length 2939-mm and an SBIG STX-16803 camera with KAF-16803 CCD detector (4096×4096, 9 μm pixels), providing a 43× 43 arcmin^2 field of view. The camera is thermo-electrically cooled and was operated at −20°C. All frames were taken with the Baader R filter; this has a performance similar to the Astrodon Sloan r' filter used by the APASS survey (Smith, Henden & Terrell 2010). The data sets were calibrated in the standard way using flat-field, dark and bias frames. Synthetic aperture photometry of the target relative to five comparison stars was performed using the software package MAXIM DL v. 5.18. The aperture radius, (≈4 arcsec), was set to twice the full-width at half-maximum of the stellar profiles in each image.

3.2 Spectroscopy

Spectroscopy of WASP 0845+53 was obtained with the ISIS spectrograph on the 4.2-m William Herschel Telescope (WHT) at the Observatorio del Roque de los Muchachos on the nights 2010 April 23–26. We used the R600B grating on the blue arm to obtain spectra covering the wavelength range 3650–5100 Å at a dispersion of 0.44 Å pixel^{-1}. The exposure time was 600 s and the signal-to-noise ratio in a typical spectrum as approximately 150 per pixel. Spectra were extracted from the images using the software package PAMELA and the spectra were analysed using the program MOLLY.[1] Observations of the star were bracketed by calibration arc observations and the wavelength calibration interpolated to the time of mid-observation for each spectrum. The rms residual of a fourth order polynomial fit to the 33 arc lines used for the wavelength calibration was typically 0.02 Å. The resolution of the spectra is approximately 1.1 Å.

Spectroscopy of WASP 0843−11 and WASP 1323+43 was obtained with the Sandiford Cassegrain Echelle Spectrometer (SES) on the 2.1-m Otto Struve Telescope at McDonald Observatory on the nights 2012 January 04–16. The exposure time used was 1800 s. The mean dispersion is 0.037 Å pixel^{-1} and the resolving power of the spectrograph is $R \approx 60\,000$. The typical signal-to-noise ratio per pixel is approximately 25 for WASP 1323+43 and 5 for WASP 0843−11. These spectra cover the wavelength range 4011–4387 Å. The spectra were reduced using IRAF.[2]

Spectroscopy of WASP 1323+43, WASP 1625−04, WASP 1628+10 and WASP 2101−06 was obtained using the Twin spectrograph on the 3.5-m telescope at the Calar Alto observatory. We used the T12 600 line/mm grating in the blue arm to obtain spectra covering the approximate wavelength range 3290–5455 Å at a dispersion of 1.1 Å pixel^{-1}. Spectra were extracted from the images using the software package PAMELA and the spectra were analysed using the program MOLLY. The resolution of the spectra is approximately 2.3 Å. The rms residual of a third order polynomial fit to the 15 arc lines used for the wavelength calibration was typically 0.65 Å.

4 ANALYSIS

4.1 Light-curve analysis

We used JKTEBOP[3] (Southworth 2010 and references therein) to analyse the WASP and PIRATE light curves using the EBOP light-curve model (Etzel 1981; Popper & Etzel 1981). The parameters of the model are: the surface brightness ratio $J = S_{\rm B}/S_{\rm A}$, where $S_{\rm A}$ is the surface brightness of star A ('the primary star') and similarly for star B ('the secondary star');[4] the sum of the radii relative to semi-major axis, $s = (R_{\rm A} + R_{\rm B})/a$; the ratio of the radii, $k = R_{\rm B}/R_{\rm A}$; the orbital inclination, i; the orbital period, P; the UTC time (HJD) of the centre of the eclipse of star B, T_0; the mass ratio, $q = M_{\rm B}/M_{\rm A}$; the linear limb-darkening coefficient for star A, $x_{\rm A}$. We define star

[1] deneb.astro.warwick.ac.uk/phsaap/software

[2] IRAF is distributed by the National Optical Astronomy Observatory, which is operated by the Association of Universities for Research in Astronomy (AURA) under cooperative agreement with the National Science Foundation.

[3] www.astro.keele.ac.uk/∼jkt/codes/jktebop.html

[4] More precisely, JKTEBOP uses the surface brightness ratio for the stars calculated at the centre of the stellar discs, but for convenience we quote the mean surface brightness ratio here.

Table 2. Parameters for the light-curve models fit by least-squares. L_B/L_A is the luminosity ratio in the band noted; other parameter definitions are given in the text. T_0 is given as HJD(UTC)-245 0000 and N is the number of observations. See Section 4.1.1 for a discussion of possible systematic errors in these parameters.

Star band	T_0 ±	P (d) ±	J ±	i ±	s ±	k ±	x_A ±	q ±	R_A/a ±	R_B/a ±	L_B/L_A ±	N rms
WASP 0131+28	4053.3730	1.882752	1.239	86.5	0.2710	0.2904	0.34	0.075	0.2100	0.0610	0.1058	13590
WASP	0.0003	0.000001	0.014	0.4	0.0025	0.0017	0.04	0.045	0.0019	0.0007	0.0011	0.010
WASP 0346−21	5178.3330	0.9285752	2.749	79.1	0.4278	0.1720	0.40	0.165	0.3650	0.0628	0.0800	22163
WASP	0.0002	0.0000003	0.073	0.5	0.0048	0.0021	0.09	0.035	0.0042	0.0009	0.0007	0.008
WASP 0358−31	4148.9483	2.189309	3.35	84.5	0.2944	0.1294	0.67	0.119	0.2606	0.0337	0.0559	6770
WASP	0.0009	0.000008	0.14	1.6	0.0094	0.0029	0.14	0.021	0.0082	0.0014	0.0007	0.008
WASP 0843−11	4846.8921	0.792833	2.468	75.6	0.5129	0.1591	0.48	0.176	0.4425	0.0704	0.0602	5070
WASP	0.0003	0.000005	0.087	0.8	0.0074	0.0028	0.10	0.012	0.0064	0.0015	0.0010	0.007
WASP 0845+53	4808.7689	0.844143	2.45	90.0	0.3423	0.1311	0.48	0.219	0.303	0.0397	0.0415	11689
WASP	0.0004	0.000003	0.22	3.3	0.0156	0.0058	0.22	0.034	0.013	0.0028	0.0019	0.026
WASP 0939−19	5568.0975	1.0731807	2.70	75.4	0.5159	0.1515	0.44	0.144	0.4480	0.0679	0.0592	28257
WASP	0.0005	0.0000008	0.13	0.9	0.0084	0.0041	0.13	0.017	0.0075	0.0019	0.0013	0.017
WASP 1009+20	4075.5706	1.39442	1.50	83.0	0.423	0.2188	0.43	0.135	0.347	0.0759	0.0707	3871
WASP	0.0009	0.00001	0.11	2.9	0.018	0.0084	0.21	0.032	0.014	0.0046	0.0030	0.022
WASP 1021−28	4159.5203	0.9008980	2.447	82.1	0.4474	0.2070	0.47	0.143	0.3707	0.0767	0.1026	15912
WASP	0.0003	0.0000002	0.050	0.6	0.0041	0.0021	0.06	0.027	0.0034	0.0010	0.0011	0.011
WASP 1323+43	4230.5558	0.795629	2.20	80.3	0.410	0.1856	0.52	0.192	0.346	0.0641	0.0749	5145
WASP	0.0005	0.000008	0.12	1.8	0.014	0.0053	0.20	0.039	0.012	0.0030	0.0023	0.009
WASP 1429−24	4287.0364	2.173523	2.367	80.9	0.3672	0.2337	0.49	0.136	0.2977	0.0696	0.1284	14345
WASP	0.0007	0.000002	0.066	0.5	0.0058	0.0039	0.11	0.041	0.0046	0.0016	0.0025	0.015
WASP 1625−04	4973.3928	1.5263234	2.081	82.5	0.2786	0.1702	0.50	0.126	0.2381	0.0405	0.0600	30610
WASP	0.0003	0.0000009	0.037	0.3	0.0029	0.0016	0.06	0.026	0.0025	0.0005	0.0005	0.008
WASP 1628+10	4921.8532	0.7203633	1.794	73.7	0.4878	0.2270	0.84	0.097	0.3976	0.0902	0.0935	30131
WASP	0.0005	0.0000009	0.088	0.6	0.0083	0.0044	0.16	0.019	0.0066	0.0023	0.0026	0.042
WASP 1628+10	6100.3682	0.7203633	1.90	72.9	0.491	0.209	0.31	0.092	0.4057	0.0849	0.0826	480
PIRATE	0.0004	(fixed)	0.17	0.8	0.010	0.009	0.40	0.022	0.0098	0.0029	0.0024	0.006
WASP 1814+48	4717.0636	1.7994305	3.000	90.0	0.2813	0.0964	0.59	0.134	0.2565	0.0247	0.0277	48841
WASP	0.0001	0.0000005	0.064	1.3	0.0028	0.0010	0.05	0.015	0.0025	0.0004	0.0002	0.007
WASP 2047+04	4797.7220	1.563143	1.257	80.8	0.4994	0.2379	0.50	0.102	0.4034	0.0960	0.0709	30979
WASP	0.0002	0.000001	0.033	1.2	0.0088	0.0033	0.06	0.023	0.0066	0.0024	0.0014	0.014
WASP 2101−06	4971.4605	1.2908592	2.205	89.4	0.2940	0.1470	0.52	0.130	0.2543	0.0373	0.0473	29238
WASP	0.0002	0.0000008	0.064	1.6	0.0090	0.0038	0.07	0.026	0.0067	0.0024	0.0017	0.013
WASP 2249−69	5408.1882	1.162553	1.386	79.2	0.5609	0.2530	0.51	0.148	0.4477	0.1133	0.0862	18914
WASP	0.0005	0.000003	0.040	1.2	0.0094	0.0033	0.09	0.026	0.0071	0.0026	0.0020	0.032
WASP 2328−39	4681.9316	0.7687015	1.940	81.6	0.4429	0.2984	0.49	0.252	0.3411	0.1018	0.1730	17086
WASP	0.0004	0.0000003	0.079	0.9	0.0088	0.0057	0.15	0.074	0.0067	0.0027	0.0051	0.052

B to be the smaller star in the binary in each case. We assumed that the orbit is circular and adopted a value $x_B = 0.5$ for the linear limb-darkening coefficient of star B. Varying the value of x_B has a negligible effect on the light curve. Claret & Bloemen (2011) have calculated the gravity darkening coefficient, y, for stars in the Kepler pass-band, which is similar to the WASP pass-band. The value of y varies strongly and non-monotonically over the effective temperature range of interest between the values 0.1 and 0.8. The gravity darkening coefficient of the secondary star has a negligible effect on the light curve so we set it to the value $y_B = 0.5$. It is not possible to determine the gravity darkening coefficient of the primary star, y_A, independently from the light curve because it is strongly correlated with the value of q, so we include y_A as a free parameter in the least-squares fit but limit this parameter to the range $y_A = 0.1$–0.8. We used the cyclic residual permutation method (prayer-bead method) to estimate the standard errors on the light-curve parameters. The results are given in Table 2. The observed light curves and the model fits are shown in Fig. A1.

4.1.1 Systematic errors in light-curve parameters

The mass ratio estimated from the light curve depends on the amplitude of the ellipsoidal effect, i.e. the variation between the eclipses caused by the gravitational distortion of the stars, particularly the primary star. The amplitude of the ellipsoidal effect also depends on the assumed rotation rate for the primary star. We have assumed that the primary star rotates synchronously, but this is known not to be the case in WASP 0247−25. Indeed, the mass ratio inferred from the light-curve solution for WASP 0247−25 ($q = 0.121 \pm 0.005$) is significantly different from the correct value measured directly using spectroscopy ($q = 0.137 \pm 0.002$). A similar discrepancy was observed by Bloemen et al. (2012) in the case of KOI-74, an A-star with a low-mass white dwarf companion in a 5.2-d orbit.

In the case of WASP 1628+10 we can compare the results derived from the PIRATE photometry to the results derived from the WASP photometry in order to estimate the likely level of systematic errors on the parameters. WASP 1628+10 is one of our fainter targets and there are several stars 1–2 mag fainter within a few arcmin of this star. It is unlikely that these are bright enough to significantly affect the WASP photometry. The value of s derived from the WASP light curve agrees well with the value derived from the PIRATE light curve, as might be expected given that this parameter is determined mainly by the duration of the eclipses. However, there is disagreement just below the 2σ level in the value of k derived from the two light curves. It is also possible that one, or both, of the stars in WASP 1628+10 is a pulsating star, as is the case for WASP 0247−25 A (an SX Phe-type star) and WASP 0247−25 B. The WASP photometry is obtained over many pulsation cycles and so the effect of any pulsations will be 'averaged-out' in these light curves. The same does not apply to the PIRATE light curve because some parts of the eclipses have only been observed once or twice. So, if pulsations are present then there may be a systematic error in the value of k derived from the PIRATE light curve. In principle, systematic errors in the estimation of the sky background level can affect the measured amplitude of features in the light curve such as the eclipses and the ellipsoidal effect. In practice, the typical sky background level in the WASP and PIRATE images is too low for this to be the main cause of the discrepancy. The WASP photometry is processed using the SYSREM algorithm (Tamuz, Mazeh & Zucker 2005). We inspected the power spectrum of the corrections applied by this algorithm to the WASP light curve of WASP 1628+10 and found that there is negligible power at the orbital frequency or its first harmonic. Nevertheless, obtaining accurate photometry from wide-field images such as those used in the WASP survey is not straightforward, so it is also possible that the source of the discrepancy is some instrumental effect in the WASP light curve. Whatever the source of this discrepancy may be, this level of systematic error in the value of k is not large enough to affect our conclusion that the secondary star in this binary system is a pre-He-WD.

In summary, there may be systematic errors in the values of k and q derived from the WASP light curves. In the case of WASP 1628+10, the systematic error in $R_{\rm A}/a$ is no more than a few per cent, but the value of $R_{\rm B}/a$ may be in error by about 15 per cent. This is not sufficient to affect our conclusion that the secondary stars in these binary systems are pre-He-WD.

4.2 Effective temperature estimates

We have estimated the effective temperatures of the stars by comparing the observed flux distribution of each binary star to synthetic flux distributions based on the BaSel 3.1 library of spectral energy distributions (SED; Westera et al. 2002). Near-ultraviolet (NUV) and far-ultraviolet (FUV) photometry was obtained from the *GALEX* GR6 catalogue[5] (Morrissey et al. 2007). Optical photometry was obtained from the NOMAD catalogue[6] (Zacharias et al. 2004). Near-infrared photometry was obtained from the Two Micron All Sky Survey (2MASS)[7] and Deep Near Infrared Survey of the Southern Sky (DENIS)[8] catalogues (Skrutskie et al. 2006; The DENIS Consortium 2005). The assumed surface gravity has little effect on the model spectra and so we adopt nominal values of $\log g_{\rm A} = 4.0$ for the primary stars and $\log g_{\rm B} = 5.0$ for the secondary stars. For the reddening we take the values for the total line-of-sight reddening from the maps of Schlafly & Finkbeiner (2011).[9] We compared the $E(B-V)$ values derived from these maps to the values derived using Strömgren photometry for 150 A-type stars by Schuster et al. (2004). We find that the standard deviation of the difference between these values is 0.034 mag. This additional source of error is accounted for in our analysis.

We used linear interpolation to create a grid of SEDs for the primary stars covering the effective temperature range $T_{\rm eff,\,A} = 6000$–10 000 K in 25 K steps, 10 000–13 000 K in 50 K steps and 13 000–17 000 K in 100 K steps. We produced a similar grid for the secondary stars over the effective temperature range $T_{\rm eff,\,B} = 7000$ K–30 000 K. Both grids cover the metallicity range [Fe/H] = −2.0 to [Fe/H] = 0.5 in steps of 0.5.

For every pair of $T_{\rm eff,\,A}$ and $T_{\rm eff,\,B}$ values we integrated the synthetic SED of each star over a rectangular band-pass that approximates the band-pass for each of the observed flux measurements. We then combined these synthetic flux distributions according to the luminosity ratio of the stars in the WASP photometric band given in Table 2 and calculated the value of the scaling factor, z, that minimizes the quantity

$$\chi^2_{\rm f} = \sum_{i=1}^{N_{\rm f}} \frac{(f_{{\rm obs},i} - z f_{{\rm syn},i})^2}{\sigma_i^2 + (s_{\rm sys} f_{{\rm obs},i})^2},$$

where $N_{\rm f}$ is the number of flux measurements included in the fit, $f_{{\rm obs},\,i}$ are the observed flux measurements, $f_{{\rm syn},\,i}$ are the combined fluxes calculated from the synthetic SEDs and σ_i is the standard error on $f_{{\rm syn},\,i}$ given in the source catalogue. The factor $s_{\rm sys}$ is used to allow for additional uncertainties in comparing model fluxes to observed fluxes, e.g. inconsistencies between the zero-point of the flux scale from different catalogues. We included the surface brightness ratio measured from the WASP light curve as an additional constraint in the least-squares fit by using the figure of merit

$$\chi^2 = \chi^2_{\rm f} + \chi^2_J = \chi^2_{\rm f} + \frac{(J_{\rm obs} - J_{\rm syn})^2}{\sigma_J^2 + (s_{\rm sys} J_{\rm obs})^2},$$

where $J_{\rm obs}$ and σ_J are taken from Table 2 and $J_{\rm syn}$ is the surface brightness ratio in the WASP band calculated from the synthetic SEDs. In combination with the fixed luminosity ratio this is equivalent to adding the ratio of the stellar radii as a constraint in the fit.

There are five free parameters in this least-squares fit, z, $T_{\rm eff,\,A}$, $T_{\rm eff,\,B}$ and the value of [Fe/H] for each star. We fit [Fe/H] independently for each star because the primary stars may be chemically peculiar stars, e.g. Am-type stars, and the secondary stars may also have unusual surface chemical composition as a result of their evolution or diffusion of elements in their atmospheres due to gravitational settling and radiative levitation. The values of [Fe/H] that provide the best fit to these broad-band flux measurements are unlikely to be an accurate estimate of the stars' true surface composition and so we do not quote them here. We have used the value $s_{\rm sys} = 0.05$ for all the fits because this gives $\chi^2 \approx N_{\rm f} - N_{\rm par}$, where $N_{\rm par} = 5$ is the number of free parameters in the least-squares fit.

[5] galex.stsci.edu/GR6

[6] www.nofs.navy.mil/data/fchpix

[7] www.ipac.caltech.edu/2mass

[8] cdsweb.u-strasbg.fr/denis.html

[9] ned.ipac.caltech.edu/forms/calculator.html

Table 3. Effective temperature estimates based on fitting the observed flux distribution and the surface brightness ratio from the fit to the WASP light curve. $N_{\rm f}$ is the number of flux measurements included in our least-squares fits. We have assumed an error in $E(B-V)$ of ±0.034 and accounted for this additional uncertainty in the error estimates quoted for $T_{\rm eff,\,A}$ and $T_{\rm eff,\,B}$.

Star	$E(B-V)$	$T_{\rm eff,\,A}$	$T_{\rm eff,\,B}$	χ^2	χ^2_J	$N_{\rm f}$	Notes
WASP 0131+28	0.069	9500 ± 700	10 500 ± 2000	5.5	0.00	10	a,b
WASP 0346−21	0.057	7400 ± 200	9950 ± 400	12.5	0.02	12	b,c
WASP 0358−31	0.006	7600 ± 300	12 000 ± 2000	2.9	0.00	9	c,d
WASP 0843−11	0.043	6900 ± 150	9300 ± 200	7.9	0.00	12	
WASP 0845+53	0.026	8000 ± 400	15 000 ± 1800	4.5	0.02	9	
WASP 0939−19	0.063	7150 ± 250	10 150 ± 100	3.2	0.13	8	
WASP 1009+20	0.025	8600 ± 400	10 800 ± 700	5.9	0.00	10	
WASP 1021−28	0.064	7300 ± 300	9800 ± 500	0.2	0.00	8	a
WASP 1323+43	0.021	8250 ± 350	12 000 ± 900	6.3	0.00	9	c
WASP 1429−24	0.088	7150 ± 200	9700 ± 300	3.8	0.15	14	a
WASP 1625−04	0.226	9500 ± 500	11 500 ± 1500	4.6	0.00	12	b,c
WASP 1628+10	0.056	7200 ± 300	9200 ± 250	3.0	0.01	9	
WASP 1814+48	0.039	8000 ± 300	12 500 ± 1800	8.0	0.00	10	a
WASP 2047+04	0.075	8300 ± 500	9000 ± 1700	3.5	0.00	8	
WASP 2101−06	0.046	9000 ± 200	13 500 ± 1000	1.0	0.00	9	a
WASP 2249−69	0.026	7400 ± 200	8800 ± 100	4.2	0.65	11	
WASP 2328−39	0.017	7500 ± 450	9400 ± 450	1.8	0.01	11	

a. *GALEX* NUV flux measurement(s) included in fit with low weight.
b. *GALEX* FUV flux measurement(s) included in fit with low weight.
c. *GALEX* NUV flux measurement(s) excluded from fit.
d. *GALEX* FUV flux measurement(s) excluded from fit.

The saturation limits for the *GALEX* instrument are not precisely defined so for measurements close to the nominal saturation limit we increased the standard error by a factor of 10, rather than simply excluding measurements near this limit. This was particularly useful in the case of WASP 0131+28 where the *GALEX* fluxes were strongly under-predicted by the models if they were completely excluded from the fit. The fits to the observed flux distributions are shown in Fig. A2. The values of $T_{\rm eff,\,A}$, $T_{\rm eff,\,B}$ derived are given in Table 3.

We tested our method using the light-curve solution for the WASP data of XY Cet by Southworth et al. (2011). Using the same method as described above we derive effective temperatures $T_{\rm eff,\,A} = 7865 \pm 610$ K and $T_{\rm eff,\,B} = 7360 \pm 500$ K. While these values are not very precise, they are in good agreement with the values $T_{\rm eff,\,A} = 7870 \pm 115$ K and $T_{\rm eff,\,B} = 7620 \pm 125$ K derived from the analysis of the spectra of these stars.

4.3 Spectral types

We have estimated the spectral types of our target stars by comparing the hydrogen lines and other spectral features[10] in our-low resolution spectra to the spectra of bright stars with known spectral types (Fig. 1). The spectral types derived are listed in Table 4. These spectral types apply to the combined spectrum of the binary. The optical spectrum is dominated by the light from star A and so the spectral type of star A in each binary will be very similar to the value given in Table 4 unless star B has a very unusual spectrum. We did not notice any obvious signs of chemical peculiarity in these spectra. The Ca II K lines in some targets are slightly weak compared to those in the standard stellar spectra, which may be an indication of chemical peculiarity, but this line varies rapidly with spectral type so this is not a strong indication in this case. In the two cases where spectral types are listed in SIMBAD for our targets our spectral types are later than the published values by two sub-types.

[10] ned.ipac.caltech.edu/level5/Gray/frames.html

4.4 Radial velocity measurements

We used a spectrum of the A4 V star HD 145689 (Bagnulo et al. 2003) as a template in a cross-correlation analysis of our spectra to measure the radial velocities of the primary star. We analysed the spectral regions 4900–5300 Å, 4370–4830 Å and 4120–4320 Å independently for WASP 0845+53 and took the mean radial velocity derived from the peak of the cross-correlation function. For WASP 1323+43 we analysed the entire spectrum excluding a 40 Å region around each Balmer line. The radial velocities derived and corrected for the radial velocity of the template taken from the SIMBAD data base (-9 km s^{-1}) are listed in Table 5. The standard errors given in Table 5 were found by requiring the reduced chi-squared value of a circular orbit fit to be $\chi^2_r = 1$. The parameters of the circular orbit fits are given in Table 6 and the fits are shown in Fig. 2.

We attempted a similar analysis of the spectra obtained with the Twin spectrograph but found that the radial velocities derived were only accurate to about ±20 km s^{-1}. We obtained one or two spectra near each of the quadrature phases, so these data are sufficient to show that WASP 1625−04 B, WASP 1628+10 B and WASP 2101−06 B are low-mass objects ($\lesssim$0.3 M$_\odot$), but are not accurate enough to make a useful estimate of these stars' masses. The radial velocities derived from the McDonald spectra of WASP 0843−11 are also affected by systematic errors due to problems in combining data from different echelle orders in these low signal-to-noise ratio spectra. Again, we can confirm that WASP 0843−11 B is a low-mass star ($\lesssim$0.3 M$_\odot$) but are not able to reliably estimate its mass.

4.5 Kinematics

We have calculated the Galactic U, V, W velocity components for the stars in our sample with measured radial velocities. For WASP 0845+53 and WASP 1323+43 we use the centre-of-mass

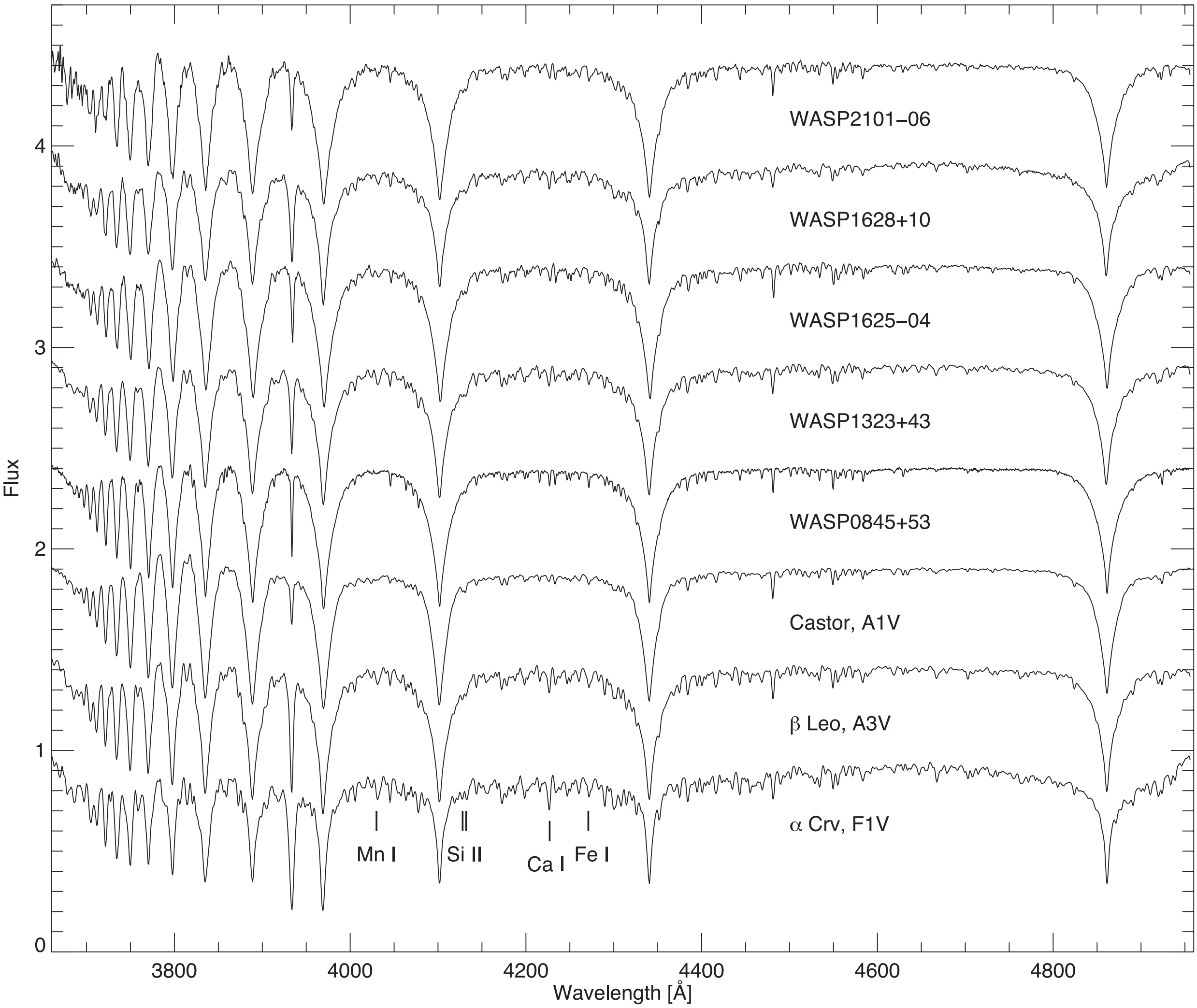

Figure 1. Spectra of five EL CVn-type binary stars compared to three stars of known spectral type, as labelled (Sánchez-Blázquez et al. 2006). The spectra are offset by multiples of 0.5 units for clarity. The Si II feature is enhanced in Ap- and Am-type stars. The other spectral features indicated are useful for assigning spectral type for A-type stars.

Table 4. Spectral types, radial velocities, proper motions and distances for new EL CVn binaries.

Star	Spectral type This paper	Spectral type SIMBAD	V_r (km s^{-1})	μ_α (mas yr^{-1})	μ_δ (mas yr^{-1})	d (pc)
WASP 0358−31		A3	-2 ± 20	1.4 ± 1.0	-3.5 ± 1.0	535 ± 40
WASP 0843−11			24 ± 11	-11.1 ± 1.0	8.1 ± 1.0	410 ± 30
WASP 0845+53	A2 V		-42 ± 2	-6.4 ± 1.0	-46.1 ± 1.6	1200 ± 100
WASP 1323+43	A3 V	A1 V	-58.6 ± 0.3	19.5 ± 0.5	-18.8 ± 0.5	280 ± 20
WASP 1625−04	A2 V	A0	9 ± 4	6.3 ± 1.0	2.5 ± 1.0	410 ± 30
WASP 1628+10	A2 V		-59 ± 20	-14.1 ± 1.1	1.8 ± 1.1	1040 ± 80
WASP 2101−06	A2 V		-12 ± 16	-4.1 ± 1.0	-15.4 ± 1.0	800 ± 60

velocity and its standard error from Table 6. The radial velocity of WASP 0358−31 is taken from Siebert et al. (2011), but rather than the quoted standard error we use a nominal standard error of 20 km s^{-1} to account for the unknown contribution of the orbital velocity to this measurement. For the other stars we use the mean radial velocity and its standard error measured from the Twin spectra. For the proper motions of the stars we used the average of the results from the PPMXL, UCAC4 and NOMAD catalogues (Roeser, Demleitner & Schilbach 2010; Zacharias et al. 2013, 2004). The proper motion values in these catalogues are not independent so we assigned an error of 1 mas yr^{-1} to these values or used the standard error of the mean if this is larger. To estimate the distance we assumed that the primary star has a mass in the range 1–2 M$_\odot$ and then used the values of P, q and $R_{\rm A}/a$ from Table 2 to estimate the radius of this star. We then used the 2MASS apparent K-band magnitude corrected for the contribution from the secondary star and the calibration of K-band surface brightness as a function of effective temperature from Kervella et al. (2004) to estimate the

Table 5. Radial velocity measurements.

Star	HJD -2450000	V_r (km s^{-1})	Source
WASP 0845+53	5310.3621	-8.8 ± 3.8	WHT, ISIS
	5311.3687	-18.9 ± 3.8	WHT, ISIS
	5311.3759	-20.2 ± 3.8	WHT, ISIS
	5312.3903	-68.5 ± 3.8	WHT, ISIS
	5312.3975	-60.0 ± 3.8	WHT, ISIS
	5313.3539	-81.9 ± 3.8	WHT, ISIS
	5313.3611	-82.3 ± 3.8	WHT, ISIS
WASP 1323+43	5937.9794	-57.4 ± 1.3	McDonald
	5938.0028	-55.7 ± 1.3	McDonald
	5938.0259	-48.6 ± 1.3	McDonald
	5941.0084	-85.1 ± 1.3	McDonald
	5941.0318	-83.8 ± 1.3	McDonald
	5942.9687	-30.4 ± 1.3	McDonald
	5942.9900	-30.7 ± 1.3	McDonald
	5943.0161	-35.4 ± 1.3	McDonald
	5930.9816	-29.5 ± 1.3	McDonald
	5931.0052	-28.5 ± 1.3	McDonald
	5931.0285	-29.2 ± 1.3	McDonald
	5932.9999	-88.6 ± 1.3	McDonald
	5933.0236	-85.9 ± 1.3	McDonald
	5934.0083	-55.6 ± 1.3	McDonald
	5934.0298	-51.9 ± 1.3	McDonald

Table 6. Parameters for least-squares fits of a circular orbit to our measured radial velocities, $V_r = V_0 + K \sin((t - T_0)/P)$. The values of T_0 and P are taken from Table 2 and $f_{\rm m}$ is the mass function.

Star	V_0 (km s^{-1})	K (km s^{-1})	$f_{\rm m}$ (M$_\odot$)
WASP 0845+53	-42.2 ± 1.5	38.0 ± 1.8	0.0048 ± 0.0007
WASP 1323+43	-58.6 ± 0.3	29.0 ± 0.4	0.0020 ± 0.0001

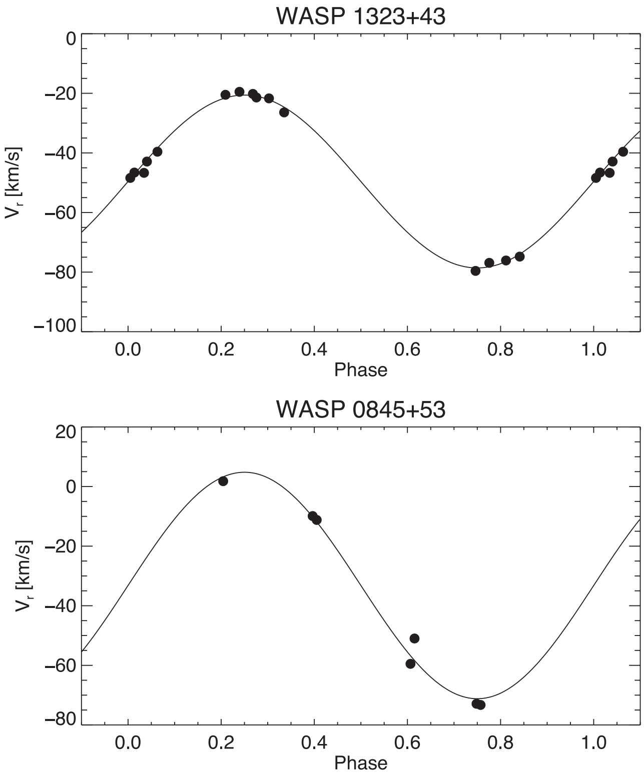

Figure 2. Measured radial velocities as a function of orbital phase for WASP 1323+43 and WASP 0845+53 (points) with circular orbits fit by least-squares (lines).

distance to the binary. The values of U, V and W were calculated using the methods described in Pauli et al. (2006) and are given in Table 7, together with the eccentricity (e) and z-component of the angular momentum ($J_{\rm Z}$) of the systems' Galactic orbits.

Fig. 3 shows our targets in the U–V and e–$J_{\rm Z}$ diagrams. WASP 0845+53 is clearly a halo star. The e$-J_{\rm Z}$ diagram enables us to identify five thin-disk stars – these are noted in Table 7. The remaining two targets are either thin-disk or thick-disk stars. We note in passing that the position of WASP 0247−25 in the e–$J_{\rm Z}$ diagram is consistent with the assumption used in Maxted et al. (2013) that this star belongs to the thick-disk population.

4.6 Masses and radii

The surface gravity of the secondary star can be derived from the analysis of an SB1 binary with total eclipses without any assumptions about the masses or radii of the stars (Southworth et al. 2004). The effective temperatures and surface gravities of WASP 0845+53 B ($\log g = 5.32 \pm 0.07$) and WASP 1323+43 B ($\log g = 4.82 \pm 0.04$) are compared to models for the formation of low-mass white dwarfs in Fig. 4. These models predict that the masses of WASP 0845+53 B and WASP 1323+43 B are both approximately 0.19 M$_\odot$.

The mean stellar density can be estimated from the parameters given in Table 2 via Kepler's Law using the equation $\rho/\rho_\odot = 0.0134\left[(R_{\rm A}/a)^3(P/d)^2(1+q)\right]^{-1}$. We compared the effective temperature ($T_{\rm eff}$) and mean stellar density (ρ) of WASP 0845+53 A and WASP 1323+43 A to models from the Dartmouth Stellar Evolution Database (Dotter et al. 2008). A zero-age main-sequence (ZAMS) star model with solar composition and a mass of 1.75 M$_\odot$ provides a good match to WASP 1323+43 A in the ρ – $T_{\rm eff}$ plane (Fig. 5). A ZAMS model with the same composition but a slightly lower mass provides a good fit for WASP 0845+53 A. Both stars will be less massive if they have a more metal-poor composition, which may be more appropriate for the halo star WASP 0845+53. For example, WASP 0845+53 A is well matched by a model with a mass of 1.45 M$_\odot$ and a composition ([Fe/H], [α/Fe]) = (−0.5, 0.2) for an apparent age of about 1 Gyr. Note that this is the age of a single-star model, the binary system may be much older because the A-type star will have gained mass from its companion during the formation of the pre-He-WD.

4.7 Notes on individual objects

WASP 0358−31. This star is listed in the third data release of the RAdial Velocity Experiment (RAVE) catalogue (Siebert et al. 2011). The stellar parameters from this catalogue are $T_{\rm eff} = 7647$ K, $\log g = 4.17$, [M/H] = 0.07 and [α/Fe] = 0.00. This effective temperature estimate is in good agreement with our own estimate of the primary star effective temperature based on the flux distribution of the star and light-curve solution (Table 3). It should be noted that the stellar parameters from the RAVE catalogue do not account for the contribution of the secondary star to the observed spectrum. The distance to this star estimated by Zwitter et al. (2010) based on an analysis of the RAVE spectrum (504 ± 182) is in good agreement with the value in Table 7, though less precise.

Table 7. Galactic U, V, W velocity components of the stars in our sample and WASP 0247−25. The eccentricity (e) and the z-component of the angular momentum (J_Z) of the stars' Galactic orbits are also given. The population to which each star belongs has been estimated based on the stars' positions in the U–V and e–J_Z diagrams.

Star	U (km s^{-1})	V (km s^{-1})	W (km s^{-1})	e	J_Z (kpc km s^{-1})	Population $U-V$	Population $e-J_Z$
WASP 0247−25	−91 ± 16	67 ± 26	34 ± 13	0.705 ± 0.104	643 ± 215	Thick disc	Thick disc/halo
WASP 0358−31	17 ± 2	219 ± 2	10 ± 2	0.077 ± 0.007	1905 ± 17	Disc	Thin disc
WASP 0843−11	−17 ± 2	230 ± 2	1 ± 2	0.055 ± 0.007	2008 ± 14	Disc	Thin disc
WASP 0845+53	−33 ± 6	−38 ± 19	−31 ± 4	0.841 ± 0.079	−363 ± 178	Halo	Halo
WASP 1323+43	47 ± 2	217 ± 1	−7 ± 1	0.144 ± 0.006	1848 ± 4	Disc	Thin disc
WASP 1625−04	14 ± 1	251 ± 2	2 ± 2	0.087 ± 0.007	1931 ± 12	Disc	Thin disc
WASP 1628+10	−15 ± 4	188 ± 5	62 ± 5	0.142 ± 0.017	1451 ± 42	Disc	Thin disc
WASP 2101−06	35 ± 3	170 ± 4	3 ± 3	0.232 ± 0.017	1363 ± 33	Disc	Disc

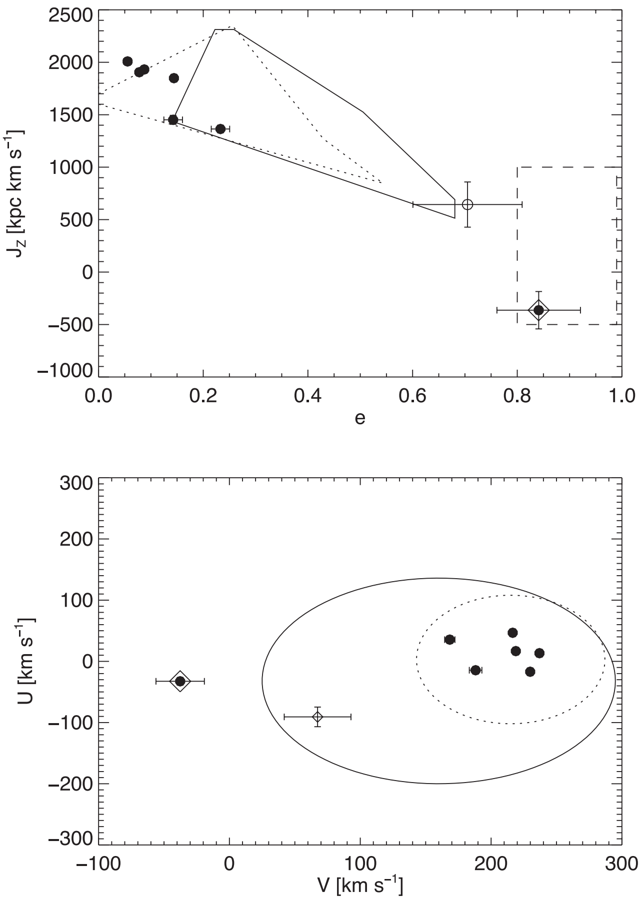

Figure 3. Upper panel: eccentricity (e) and z-component of the angular momentum (J_Z) of the Galactic orbits for our targets. The regions in which thin-disk (dotted lines), thick-disk (solid lines) and halo stars (dashed-lines) are found based on the results of Pauli et al. (2006) are indicated. Lower panel: Galactic U and V velocities of our targets. Contours are 3σ limits for the U–V distribution of main-sequence thin-disk and thick-disk stars. In both panels the open symbol shows the location of WASP 0247−25 and WASP0845+53 is highlighted with an open diamond symbol.

WASP 1323+43. The estimated distance to this star given in Table 7 is in good agreement with the parallax measured using the *Hipparcos* satellite (van Leeuwen 2007). This star was detected as a periodic variable star using the *Hipparcos* epoch photometry by Koen & Eyer (2002), although the period measured from those data was found to be incorrect by a factor of 2 by Otero & Dubovsky (2004). This star appears in two libraries of stellar spectra as a standard A1V-type star (Jacoby, Hunter & Christian 1984; Silva & Cornell 1992).

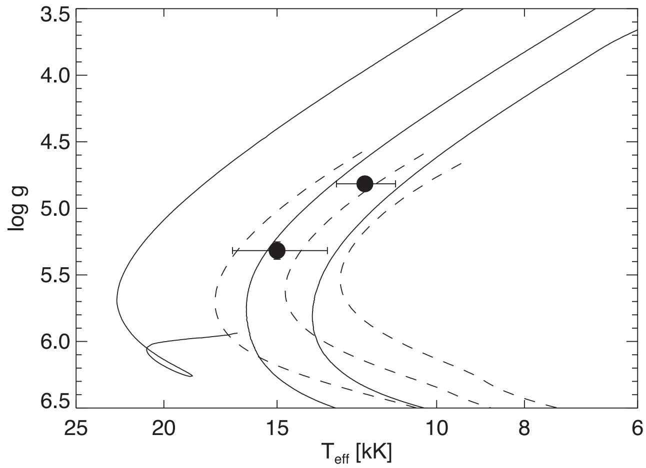

Figure 4. Effective temperature ($T_{\rm eff}$) and surface gravity ($\log g$) of WASP 0845+53 B ($T_{\rm eff}$ = 15 000 K, $\log g$ = 5.3) and WASP 1323+43 B ($T_{\rm eff}$ = 12 000 K, $\log g$ = 4.8) compared to models for the formation of low-mass white dwarfs. Solid lines show (from left to right) the models of Driebe et al. (1998) for masses 0.234 M$_{\odot}$, 0.195 M$_{\odot}$ and 0.179 M$_{\odot}$. Dashed lines show (from left to right) the models of Serenelli et al. (2002) for $Z = 0.001$ and masses 0.197 M$_{\odot}$, 0.183 M$_{\odot}$ and 0.172 M$_{\odot}$.

5 DISCUSSION AND CONCLUSIONS

The positions of WASP 0845+53 B and WASP 1323+43 B in Fig. 4 show that these are certainly pre-He-WD with masses $\approx$0.19 M$_{\odot}$. The available spectroscopy for WASP 1625−04, WASP 1628+10, WASP 2101−06 and WASP 0843−11 shows that the secondary stars in these binary systems have masses $\lesssim$0.3 M$_{\odot}$ and effective temperature ∼10 000 K, which is exactly as expected for pre-He-WDs. The minimum mass for a core helium burning star is about 0.33 M$_{\odot}$, but these anomalously low masses only occur for a narrow range of initial stellar mass around 2.3 M$_{\odot}$ (Han et al. 2002; Prada Moroni & Straniero 2009). Although our upper limit on the mass of these stars does not completely exclude the possibility that they are core helium burning stars, the following argument does make this extremely unlikely, both for these stars and for the stars for which we do not yet have any spectroscopy.

The models of Prada Moroni & Straniero (2009) show that low-mass core helium burning stars only have effective temperatures ∼10 000 K during phases when they are evolving very rapidly

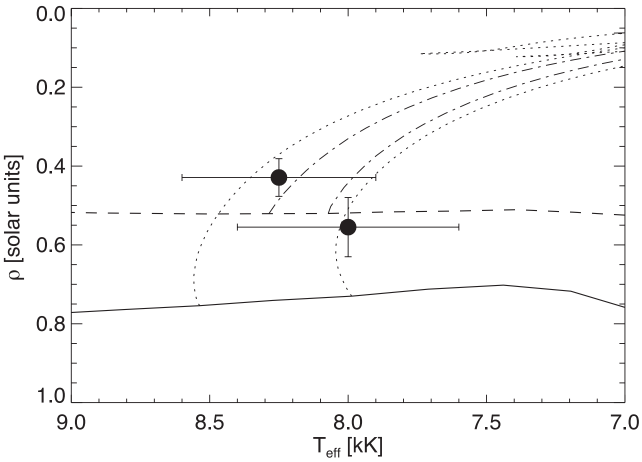

Figure 5. Mean density and effective temperature of WASP 0845+53 A ($T_{\rm eff} = 8\,000$ K, $\rho = 0.56\rho_{\odot}$) and WASP 1323+43 A ($T_{\rm eff} = 8\,250$ K, $\rho = 0.43\rho_{\odot}$) compared to the stellar models of Dotter et al. (2008). ZAMS isochrones are shown for models with ([Fe/H], [α/Fe]) = (0.0, 0.0) (short-dashed line); (−0.5, 0.2), (solid line). Evolutionary tracks are plotted as follows: (0.0, 0.0), 1.70 $M_{\odot}$ and 1.75 $M_{\odot}$ (dash–dotted line); (−0.5, 0.2), 1.45 $M_{\odot}$ and 1.5 $M_{\odot}$ (dotted lines).

or when their luminosity is $\log(L/L_{\odot}) \gtrsim 1$. If we assume that smaller star in the binary has a luminosity $\log(L_{\rm B}/L_{\odot}) = 1$ then the luminosity ratios in Table 2 and effective temperatures in Table 3 require that the larger star in these binaries have radii $R_{\rm A} \approx 5$–$10\,R_{\odot}$. These radii can be combined with the value of $R_{\rm A}/a$ from Table 2 and Kepler's Law to make an estimate of the mass of star A in each binary. We used bolometric corrections for the *V* band from Balona (1994) to convert the luminosity ratio in the WASP band from Table 2 to a bolometric luminosity ratio. We find that the assumption $\log(L_{\rm B}/L_{\odot}) = 1$ leads to masses from $12 \pm 2\,M_{\odot}$ to $115 \pm 16\,M_{\odot}$, with a typical value of $40 \pm 10\,M_{\odot}$. This is clearly much too high for the mass of an A-type star that can fit into an orbit with a period of less than 2.2 d. Nevertheless, given the current observational uncertainties (particularly for those stars without spectroscopic follow-up) it may be possible that a few of these binary systems contain stars with a small carbon–oxygen core produced during an evolutionary phase not explored by the models of Prada Moroni & Straniero.

WASP 0845+53 A is a blue-straggler, i.e. an apparently young star in an old stellar population (the Galactic halo). If we assume that the red giant progenitor of WASP 0845+53 B had a mass close to the halo turn-off mass ($\approx 0.8\,M_{\odot}$) and that this was initially the more massive star in the binary system, then we see that WASP 0845+53 A must have gained about $0.6\,M_{\odot}$ to get to a current mass of $\approx 1.45\,M_{\odot}$.

With one exception (WASP 1429−24, F0) the spectral types of the stars are all in the range A0–A4. Dwarf stars with normal compositions in this range of spectral type have $T_{\rm eff} \approx 8000$–9400 K (Boyajian et al. 2012). The effective temperatures we have estimated by fitting the stars' flux distributions are generally within this range, but for WASP 1628+10 $T_{\rm eff}$ is about 1000 K cooler than this. The spectral type expected for this star based on our estimate of $T_{\rm eff}$ is approximately A8. Similarly, WASP0346−21, is expected to have a spectral type close to F0 based on our estimate of $T_{\rm eff}$ but the published spectral type is A4 IV. If we assume that these stars have reddening $E(B - V)$ approximately 0.15 mag larger than predicted by the reddening maps, as has been observed for some other A-type stars (Schuster et al. 2004), then we find that the effective temperatures derived are in good agreement with the spectral types. If there is a discrepancy between the effective temperatures derived from our flux-fitting method and the spectral types then the atmospheric composition of these stars may be very different to any of the compositions assumed for the BaSel 3.1 library. The resolution and signal-to-noise ratio of the spectra presented here are not sufficient to explore this issue further. A detailed analysis of high-resolution spectra with good signal-to-noise ratio would help us to better understand this problem, particularly if the spectra can be obtained during primary eclipse when there is no contribution from the companion star. In addition, high-resolution spectra covering the interstellar Na I D lines can be used to make independent estimates of the reddening to these stars (Munari & Zwitter 1997).

Until the discovery of WASP 0247-25, very few pre-He-WD were known and none of these was easy to study, being either faint, or with unseen companion stars, or both (Maxted et al. 2011). Our discovery of 17 new, bright eclipsing binary systems containing these rarely observed stars opens up the possibility of studying the formation of very low-mass white dwarfs in great detail. These discoveries also show the great value of the WASP photometric archive for the discovery and study of rare and interesting types of variable star.

The large number of photometric observations and high cadence of the WASP photometry make it possible to identify the characteristic 'boxy' primary eclipse in the light curve. This feature combined with a shallower secondary eclipse due to a transit is an unambiguous signal that a short period binary star must contain a pre-He-WD or similar highly evolved star. It would not be so straightforward to identify a pre-He-WD at an earlier phase of its evolution when it is cooler than the dwarf star. Several binary systems have been identified using Kepler photometry in which an A-type or B-type star has a young, low-mass white dwarf companion, i.e. stars at a more advanced evolutionary phase than the pre-He-WDs in EL CVn-type binaries. The Kepler binary systems have orbital periods in the range 2.6–23.9 d (Rowe et al. 2010; Carter et al. 2011; Breton et al. 2012). This suggests that there are likely to be more pre-He-WD awaiting discovery in the WASP data, particularly at longer orbital periods. With a more systematic approach to discovering these binaries, it may be possible to learn more about their formation by comparing the distributions of observed properties for a more complete sample to the predictions of binary population synthesis models.

ACKNOWLEDGEMENTS

This research has made use of the SIMBAD data base, operated at CDS, Strasbourg, France. The research leading to these results has received funding from the European Research Council under the European Community's Seventh Framework Programme (FP7/2007–2013)/ERC grant agreement no 227224 (PROSPERITY), as well as from the Research Council of the University of Leuven under grant agreement GOA/2013/012. This work was supported by the Science and Technology Facilities Council (grant numbers ST/I001719/1, ST/J001384/1). SG and DS were supported by the Deutsche Forschungsgemeinschaft (DFG) through grants HE1356/49-1 and HE1356/62-1.

REFERENCES

Agüeros M. A., Camilo F., Silvestri N. M., Kleinman S. J., Anderson S. F., Liebert J. W., 2009, ApJ, 697, 283

Althaus L. G., Serenelli A. M., Benvenuto O. G., 2001, MNRAS, 323, 471

Bagnulo S., Jehin E., Ledoux C., Cabanac R., Melo C., Gilmozzi R. The ESO Paranal Science Operations Team, 2003, The Messenger, 114, 10
Balona L. A., 1994, MNRAS, 268, 119
Bloemen S. et al., 2012, MNRAS, 422, 2600
Boyajian T. S. et al., 2012, ApJ, 746, 101
Breton R. P., Rappaport S. A., van Kerkwijk M. H., Carter J. A., 2012, ApJ, 748, 115
Brown W. R., Kilic M., Hermes J. J., Allende Prieto C., Kenyon S. J., Winget D. E., 2011, ApJ, 737, L23
Carter J. A., Rappaport S., Fabrycky D., 2011, ApJ, 728, 139
Chen X., Han Z., 2003, MNRAS, 341, 662
Claret A., Bloemen S., 2011, A&A, 529, A75
Dotter A., Chaboyer B., Jevremović D., Kostov V., Baron E., Ferguson J. W., 2008, ApJS, 178, 89
Driebe T., Schoenberner D., Bloecker T., Herwig F., 1998, A&A, 339, 123
Driebe T., Blöcker T., Schönberner D., Herwig F., 1999, A&A, 350, 89
Etzel P. B., 1981, in Carling E. B., Kopal Z., eds, Photometric and Spectroscopic Binary Systems. A Simple Synthesis Method for Solving the Elements of Well-Detached Eclipsing Systems. p. 111
Giannone P., Giannuzzi M. A., 1970, A&A, 6, 309
Han Z., Podsiadlowski P., Maxted P. F. L., Marsh T. R., Ivanova N., 2002, MNRAS, 336, 449
Heber U., Edelmann H., Lisker T., Napiwotzki R., 2003, A&A, 411, L477
Holmes S. et al., 2011, PASP, 123, 1177
Iben I., Jr, Livio M., 1993, PASP, 105, 1373
Jacoby G. H., Hunter D. A., Christian C. A., 1984, ApJS, 56, 257
Kaluzny J., Rucinski S. M., Thompson I. B., Pych W., Krzeminski W., 2007, AJ, 133, 2457
Kawka A., Vennes S., 2009, A&A, 506, L25
Kazarovets E. V., Samus N. N., Durlevich O. V., Kireeva N. N., Pastukhova E. N., 2008, Inform. Bull. Var. Stars, 5863, 1
Kervella P., Thévenin F., Di Folco E., Ségransan D., 2004, A&A, 426, 297
Kilic M., Allende Prieto C., Brown W. R., Koester D., 2007, ApJ, 660, 1451
Kilic M., Brown W. R., Allende Prieto C., Kenyon S. J., Heinke C. O., Agüeros M. A., Kleinman S. J., 2012, ApJ, 751, 141
Knigge C., Dieball A., Maíz Apellániz J., Long K. S., Zurek D. R., Shara M. M., 2008, ApJ, 683, 1006
Koen C., Eyer L., 2002, MNRAS, 331, 45
Lorimer D. R., 2008, Living Rev. Relativ., 11, 8
Marsh T. R., Dhillon V. S., Duck S. R., 1995, MNRAS, 275, 828
Maxted P. F. L. et al., 2011, MNRAS, 418, 1156
Maxted P. F. L. et al., 2013, Nat, 498, 463
Morrissey P. et al., 2007, ApJS, 173, 682
Munari U., Zwitter T., 1997, A&A, 318, 269
Nelson C. A., Eggleton P. P., 2001, ApJ, 552, 664
Nelson L. A., Dubeau E., MacCannell K. A., 2004, ApJ, 616, 1124
Otero S. A., Dubovsky P. A., 2004, Inform. Bull. Var. Stars, 5557, 1
Parsons S. G., Marsh T. R., Gänsicke B. T., Drake A. J., Koester D., 2011, ApJ, 735, L30
Pauli E.-M., Napiwotzki R., Heber U., Altmann M., Odenkirchen M., 2006, A&A, 447, 173
Pietrzyński G. et al., 2012, Nat, 484, 75
Pollacco D. L. et al., 2006, PASP, 118, 1407
Popper D. M., Etzel P. B., 1981, AJ, 86, 102
Prada Moroni P. G., Straniero O., 2009, A&A, 507, 1575
Pribulla T., Rucinski S. M., 2008, MNRAS, 386, 377
Refsdal S., Weigert A., 1969, A&A, 1, 167
Roeser S., Demleitner M., Schilbach E., 2010, AJ, 139, 2440
Rowe J. F. et al., 2010, ApJ, 713, L150
Sánchez-Blázquez P. et al., 2006, MNRAS, 371, 703
Schlafly E. F., Finkbeiner D. P., 2011, ApJ, 737, 103
Schönberner D., 1978, A&A, 70, 451
Schuster W. J., Beers T. C., Michel R., Nissen P. E., García G., 2004, A&A, 422, 527
Serenelli A. M., Althaus L. G., Rohrmann R. D., Benvenuto O. G., 2002, MNRAS, 337, 1091
Siebert A. et al., 2011, AJ, 141, 187
Silva D. R., Cornell M. E., 1992, ApJS, 81, 865
Skrutskie M. F. et al., 2006, AJ, 131, 1163
Smith T. C., Henden A., Terrell D., 2010, Soc. Astron. Sci. Annu. Symp., 29, 45
Southworth J., 2010, MNRAS, 408, 1689
Southworth J., Zucker S., Maxted P. F. L., Smalley B., 2004, MNRAS, 355, 986
Southworth J., Pavlovski K., Tamajo E., Smalley B., West R. G., Anderson D. R., 2011, MNRAS, 414, 3740
Tamuz O., Mazeh T., Zucker S., 2005, MNRAS, 356, 1466
The DENIS Consortium 2005, VizieR Online Data Catalog, 2263, 0
van Kerkwijk M. H., Rappaport S. A., Breton R. P., Justham S., Podsiadlowski P., Han Z., 2010, ApJ, 715, 51
van Leeuwen F., 2007, A&A, 474, 653
Webbink R. F., 1975, MNRAS, 171, 555
Westera P., Lejeune T., Buser R., Cuisinier F., Bruzual G., 2002, A&A, 381, 524
Willems B., Kolb U., 2004, A&A, 419, 1057
Wilson D. M. et al., 2008, ApJ, 675, L113
Zacharias N., Monet D. G., Levine S. E., Urban S. E., Gaume R., Wycoff G. L., 2004, in American Astronomical Society Meeting Abstracts, Vol. 36. Bulletin of the American Astronomical Society, The Naval Observatory Merged Astrometric Data set (NOMAD). p. 1418
Zacharias N., Finch C. T., Girard T. M., Henden A., Bartlett J. L., Monet D. G., Zacharias M. I., 2013, AJ, 145, 44
Zwitter T. et al., 2010, A&A, 522, A54

APPENDIX A: ADDITIONAL FIGURES

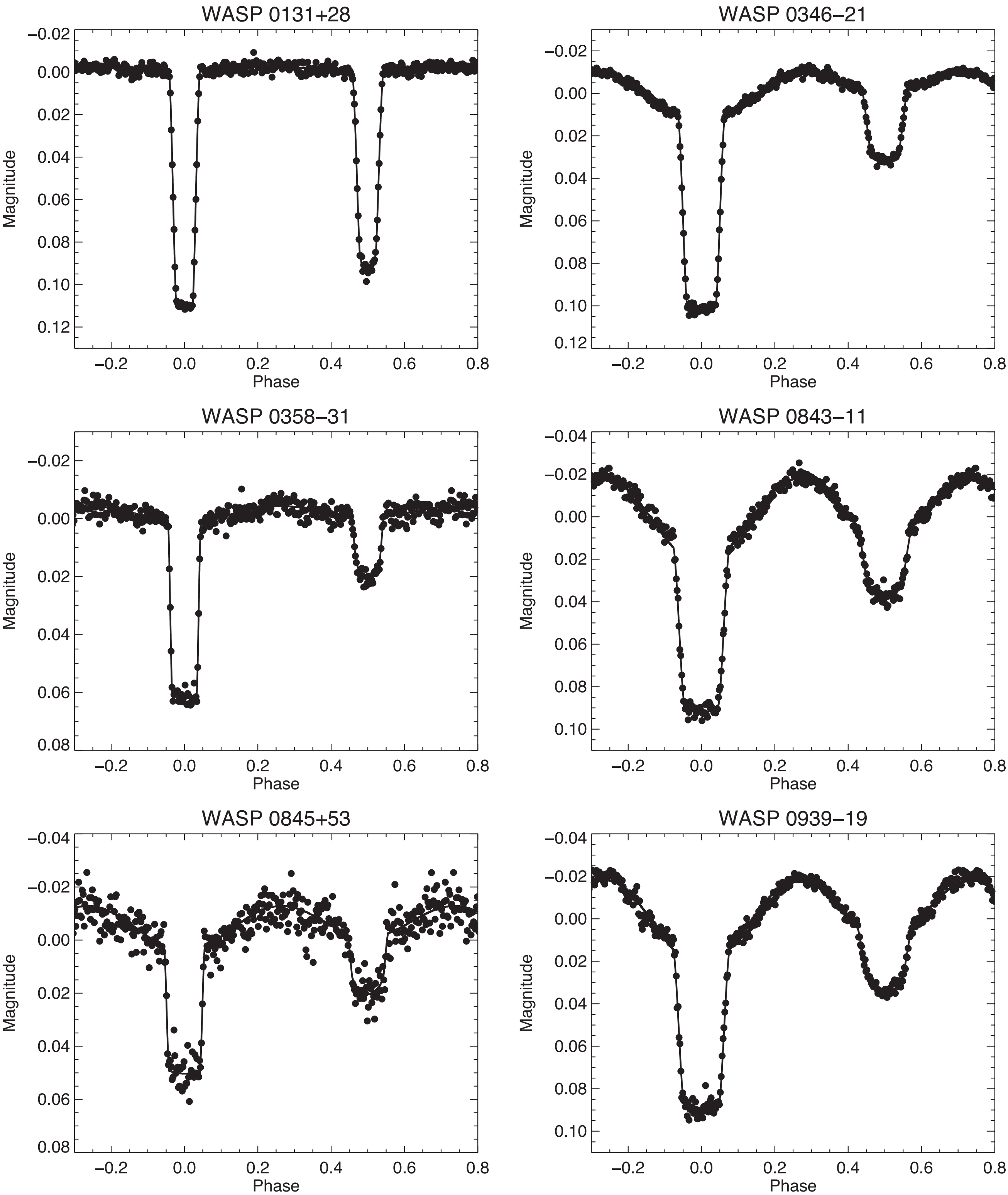

Figure A1. Observed light curves for our sample (points) with model light curves fit by least-squares (lines). The observed data have been binned in phase (bin width 0.0025) for display purposes with the exception of the PIRATE data for WASP 1628+10.

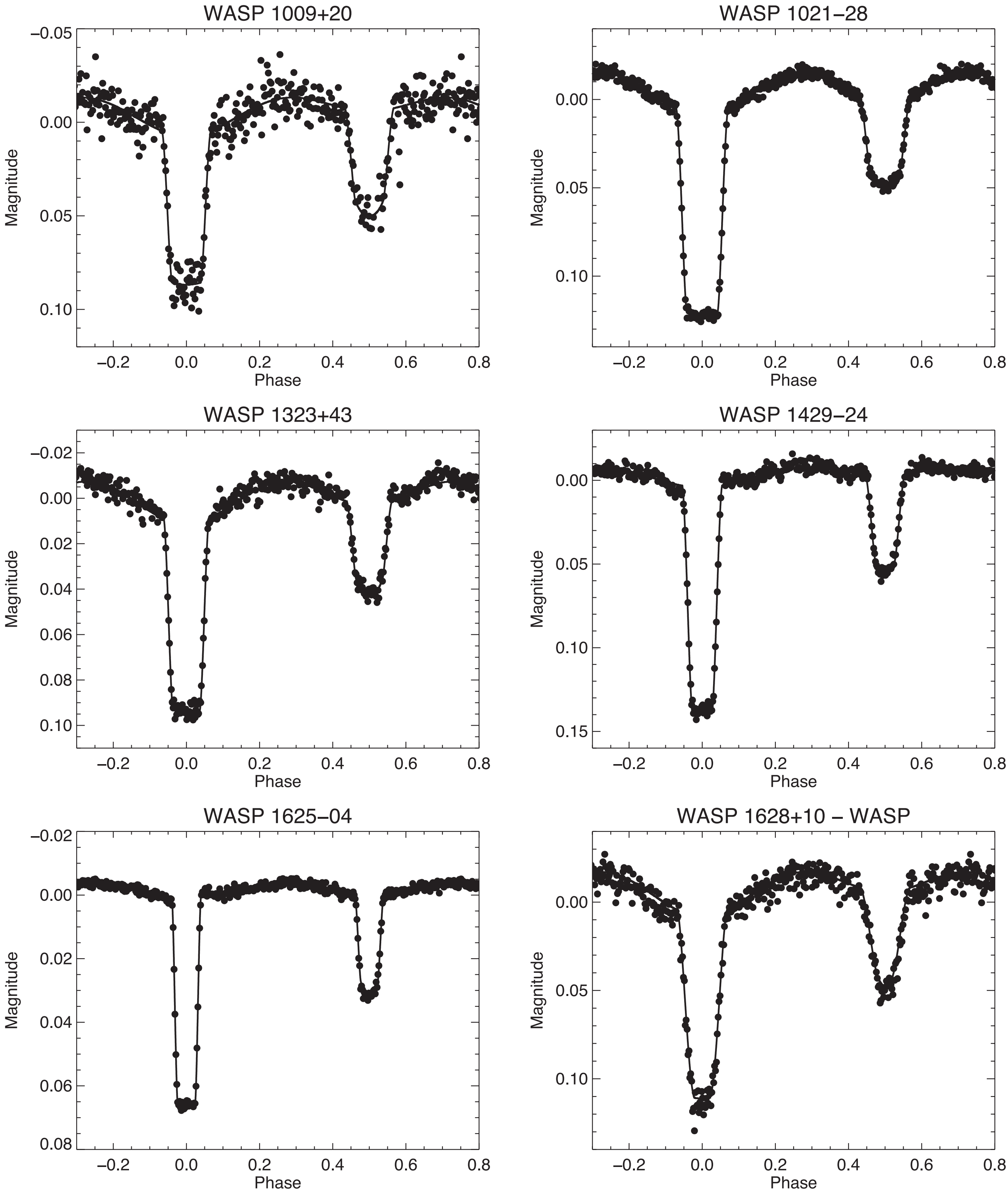

Figure A1 – *continued*

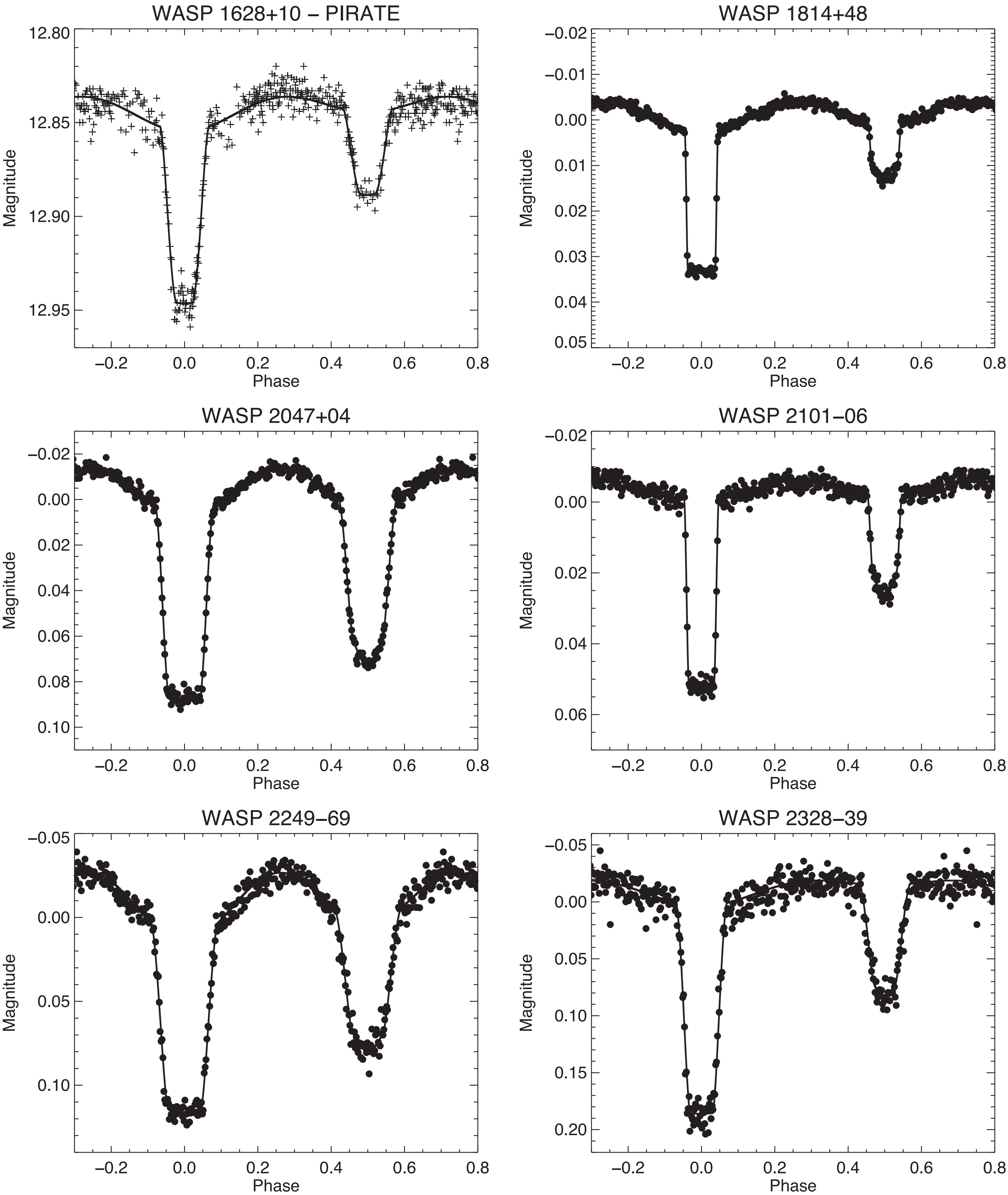

Figure A1 – *continued*

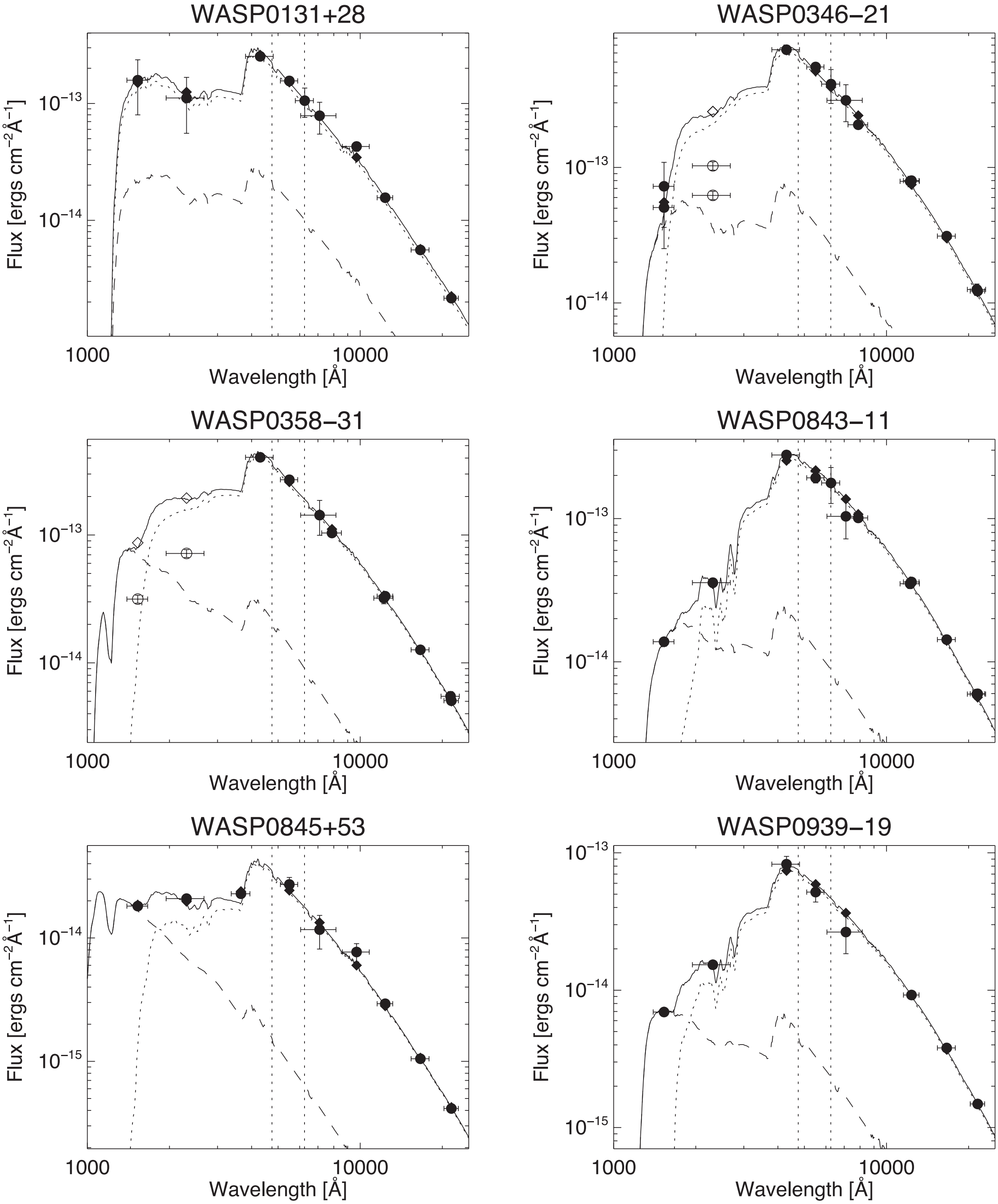

Figure A2. Model fits to the observed flux distributions used to estimate the effective temperatures of the stars in our sample. The observed fluxes are shown as circles with error bars. The predicted contributions of each star to the observed fluxes for the effective temperatures given in Table 3 are shown as dotted or dashed lines and their sum is shown as a solid line. The models have been smoothed slightly for clarity in these plots. Diamonds show the result of integrating the total model flux over the band-width indicated by horizontal error bars on the observed fluxes. Only data plotted with filled symbols were used in the least-squares fits. The assumed band-width of WASP photometry is indicated with vertical dotted lines.

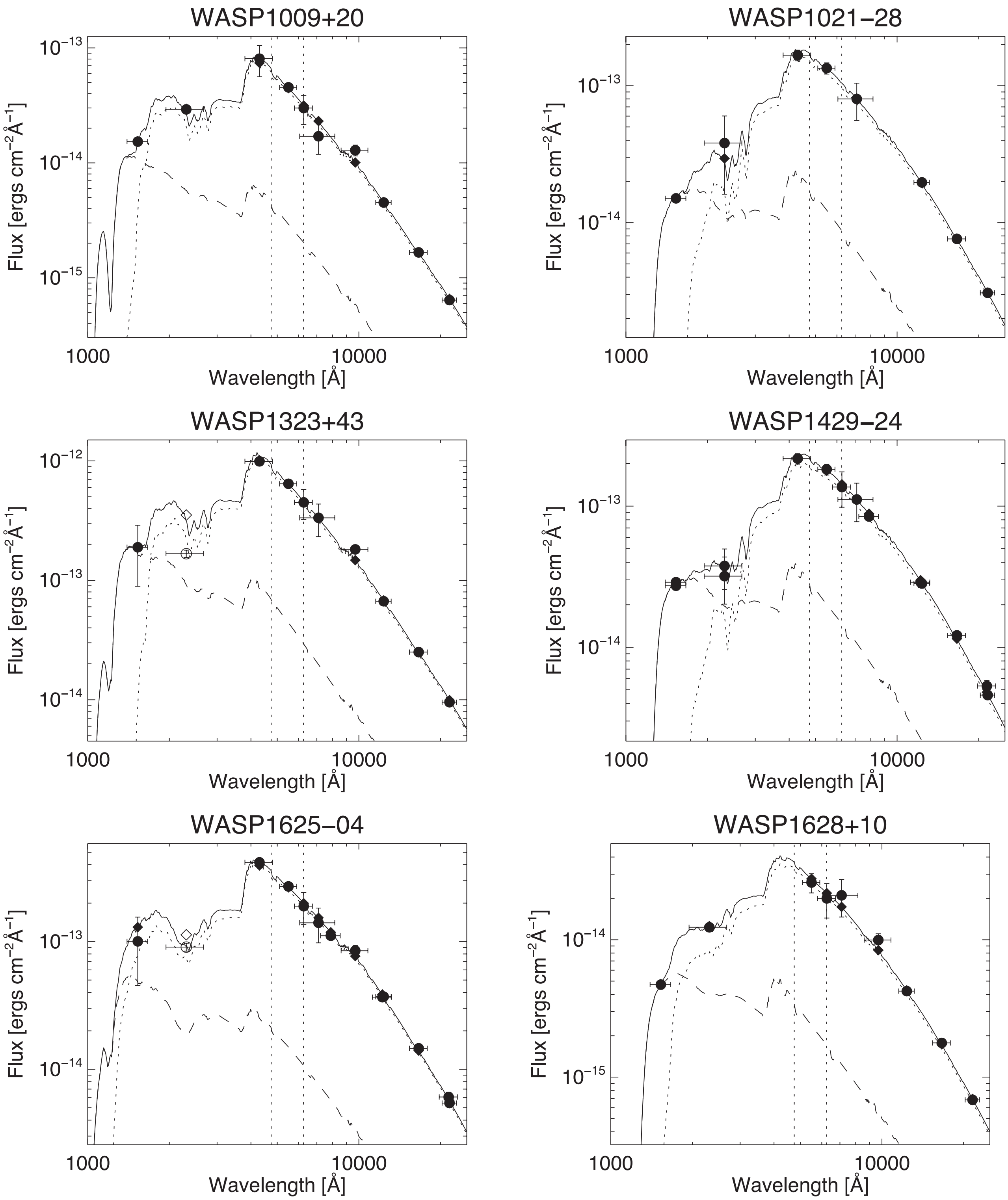

Figure A2 – *continued*

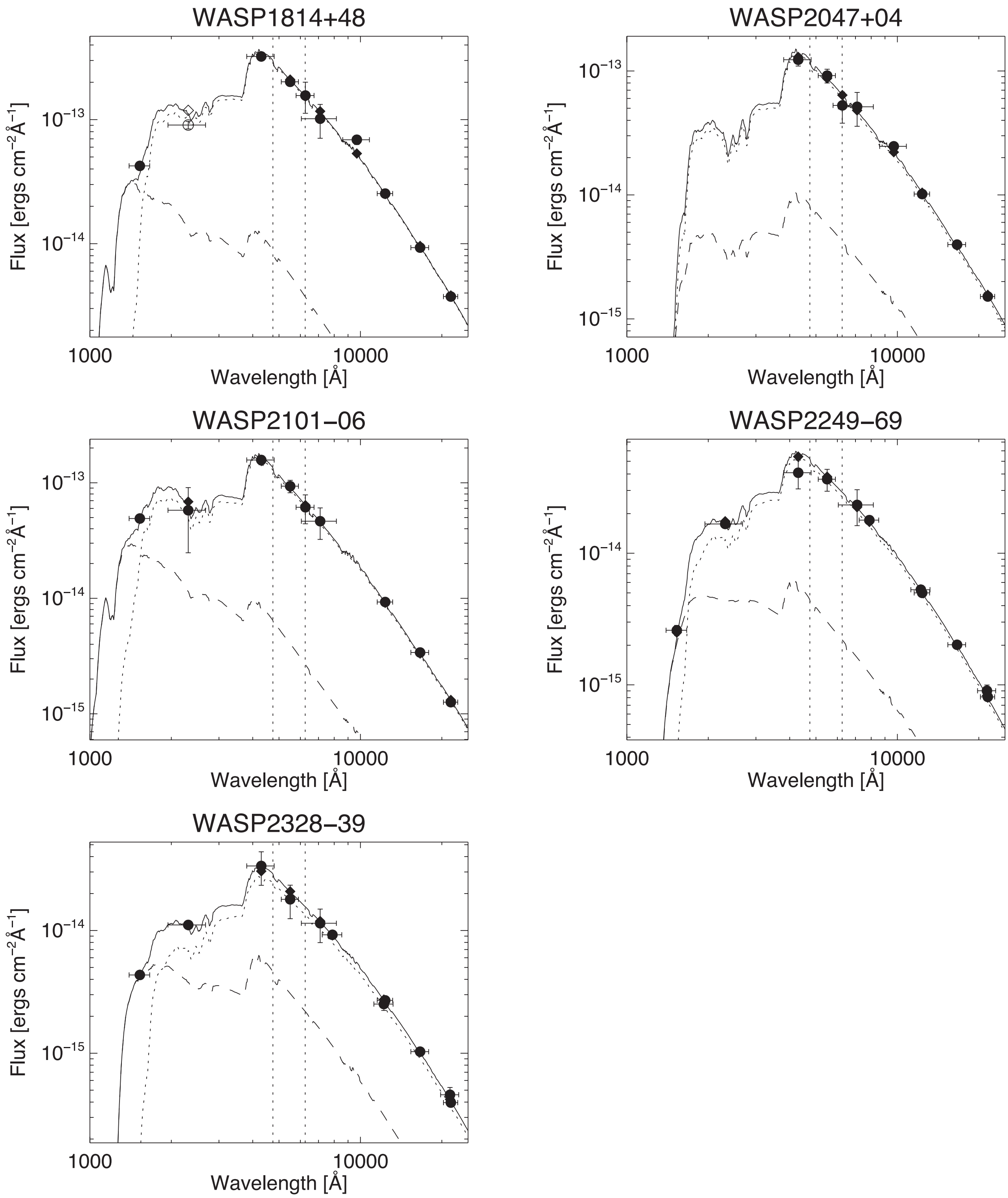

Figure A2 – *continued*

This paper has been typeset from a TEX/LATEX file prepared by the author.